Supplemental Information

SI-1. Colloidal syntheses

Samples #1 and #2 are homogeneous CdSe NRs that were prepared according to a published protocol[1] with some modifications. With the same precursors ratio, sample #1 (short NR) and sample #2 (long NR) were differently shaped by adjusting growth temperature. Sample #1 was grown at 300°C for 10 mins; Sample #2 (long and thin NR) was grown at 270°C for 10 min. Samples #3 (short NR) and #4 (long NR) are quasi type-II seeded NRs. CdSe cores and seeded CdS NRs were prepared according to published protocols ref. 2 and 3 respectively with some modifications. Their lengths were predominantly controlled by the amount of CdSe dots used for seeded growth. Samples #5 and #6 are CdTe/CdSe core/shell structured type-II QDs that were prepared by successive ion layer adsorption and reaction (SILAR) according to a published protocol[4] with some modifications. Samples #7 and #8 are type-II seeded NRs. Sample 7 has bullet-shape morphology with one ZnSe QD seed buried in CdS matrix. It was prepared according to a published protocol[5]. Sample #8 is an elongated NR having core-shell-shell structure, Te-doped CdSe core seeded in CdS (inner shell) - CdZnSe alloy (outmost shell). The detailed morphology, band structure and synthesis of sample #8 is described in ref 6.

Chemicals and materials: Cadmium oxide (CdO, 99.99%), Zinc Oxide (ZnO, 99.99%) oleic acid (90%), tri-n-octylphosphine (TOP, 90%), trioctylphosphine oxide (TOPO, 99% and technical grade 90%) hexadecylamine (HDA), octadecylamine (ODA, 97%), octylamine (97%), octadecene (ODE, 90%), tetra-butylphosphene (TBP, 97%), selenium (Se, 99.999%), telluride (Te, 99%), Sulfur (S, 99.5%) and oleylamine (OA, 70%) along with all organic solvents were purchased from Sigma-Aldrich and used without any further purification. Tetradecylphosphonic acid (TDPA), hexylphosphonic acid (HPA) and octadecylphosphonic (ODPA) were purchased from PCI Synthesis.

CdSe NRs: A three-neck flask was loaded with a mixture of 1 mmol CdO, 0.6 mmol HPA, 1.4 mmol TDPA and 2.0 g TOPO (99%). Temperature was raised slowly to 250°C under nitrogen flow to obtain clear (or slightly opaque) colorless solution. The cooled mixture was left overnight in ambient. In continuation, the mixture was reheated to 320°C under nitrogen flow. A colorless Se solution was quickly injected into this colorless solution containing 0.5 mmol Se, 0.6 mmol TBP, 2.7 mmol TOP and 0.3 g toluene. **Sample #1:** The growth temperature was set at 300°C. Due to the injection, the temperature decreased to 270°C but climbed back to 300°C within 10 mins. Growth was terminated after 10mins by rapid cooling to RT. The resulted NRs had a small aspect ratio. **Sample #2:** The same protocol as for sample #1 was followed, with two exceptions: instead of TOPO (99%), a technical grade TOPO (90%) was used, and the growth step was proceeded for 10mins at 270°C.

Quasi-Type-II NRs (CdSe seeded in CdS): CdSe core nanocrystals were prepared using a procedure modified from a previous report[2]. A 50 ml round bottom flask was loaded with 60 mg (0.5 mmol) CdO, 280 mg ODPA and 3 g TOPO. After degassing under vacuum for 1 hour at 120°C the temperature was raised to 340°C under argon until

dissolution of CdO at which point 1.8 ml TOP was injected and temperature was raised to 370°C. A solution containing 58 mg Se in 0.5 ml TOP was swiftly injected and heating mantle was removed until. Final core size had a diameter of about 2.7 nm. A slight modification of previously reported methods[7] was used for seeded growth of CdS. A 50 ml round bottom flask was charged with 211 mg (1.6 mmol) CdO, 1 g ODPA, 50 mg HPA and 3.46 g TOPO. The reaction flask was degassed for 3 hours at 130° and then temperature was raised to 340°C under argon until dissolution of CdO at which point 1.8 ml TOP was injected. CdSe seed solution was separated and purified for reaction by mixing with toluene and precipitating with excess methanol 3 times. Seeds were then re-dissolving in 0.6 ml TOP. The S:TOP precursor solution was prepared by mixing 51mg S (1.6mmol) in 0.6 ml TOP. Temperature was raised to 350°C for injection. The amount of dots used for preparation of **sample #3** was 8×10^{-7} and for **sample #4** was 1×10^{-7}moles.

Type-II QDs: CdTe/CdSe: CdTe core QDs were synthesized in high temperature organic solution. The mixture of 0.5 mmol CdO, 1.25 mmol TDPA and 20 g ODE was sonicated for 5 min before heated on the mantle to 290°C under nitrogen purging. A clear and colorless solution was obtained. Meanwhile a mixture of 0.5 mmol Te powder, 0.31 g TBP and 6 g ODE in septum-topped vial was sonicated for 5 min and then heated on a mantle to 214°C in order to dissolve the Te. This Te precursor solution, upon cooling to room temperature, was loaded into a 10 ml syringe mounted with a 12 gauge needle. Cd precursor solution was heated to 310°C under nitrogen; the Te precursor was injected into it under stirring. The temperature dropped to 270°C. At this temperature the reaction was proceeding for about 30 min (or whenever the target absorption peak position was reached). CdTe QDs were purified and characterized by UV-Vis (to estimate the concentration using known extinction coefficients) and TEM (to measure particle size and calculate surface area) for the following steps. **Sample #5:** CdTe core 4.2 nm, CdSe shell 2-monolayer, emission 670 nm. 1.2 g CdTe hexane solution (concentration was calculated in units of mmol/gram) was mixed with 0.5 g oleic acid and 3.5 g ODE in a flask. After the removal of hexane and degassing under vacuum, the flask was heated to 210°C under nitrogen. 0.04 M Cd precursor was prepared by heating to 250°C and dissolving 76.8 mg CdO in 1.35 g oleic acid and 10.65 g ODE. The colorless solution was pumped while being cooled to room temperature. Similarly 0.04 M Se precursor was made with 38 mg Se, 1.624 g TBP and 7.89 g ODE. The Cd and Se precursors were loaded into separate syringes for manual dripping or syringe pump infusion. At 210°C the first 0.104 ml Se solution was slowly dripped into the CdTe containing flask. 10 min later the same amount of Cd solution was added to complete the first monolayer of CdSe shell. For the growth of the second layer CdSe, 0.139 ml Se and Cd solutions were introduced sequentially and respectively. Successively with 0.177 ml for the third layer, 0.221 ml for the fourth and 0.270 ml for the fifth layer, the 3.9 nm CdTe QD was overcoated with 5 monolayers of CdSe, showing a single emission at 710 nm. **Sample #6:** CdTe core 3.9 nm, CdSe shell 5-monolayer, emission 710; nm. The epitaxial growth of CdSe shell onto the CdTe core was executed *via* the SILAR method[4]. Cd and Se precursor solutions were introduced into the reaction flask containing CdTe core, fresh ligands (*e.g.*, oleic acid) and solvent (ODE or TOPO) alternatively, with increasing amounts for each additional layer. The amounts were calculated to cover all QDs in solution to exact one monolayer.

Type-II NRs: ZnSe/CdS (**Sample #7)**: 3.7 nm ZnSe QD was prepared *via* multiple injections. The particles were purified by precipitations and quantified for concentration with UV-Vis[8]. 40 nmol ZnSe were redispersed in 0.7 g TOP immediately following the removal hexane by vacuum. 120 mg S were dissolved in 0.8 g hot TOP before being combined at room temperature with ZnSe/TOP for injection. Cd precursor solution was prepared by degassing the mixture of 60 mg CdO, 290 mg ODPA, 80 mg HPA and 3.0 g TOPO (Tech.) at 150°C under vacuum before the reaction with sulfur precursor in the presence of the seed (template) at 365°C. Upon the quick injection, the temperature dipped to 320°C. Without change of the setting, the temperature went back up to 365°C. The growth was stopped at 10 min after injection.

Te doped CdSe core in CdS-CdZnS-CdZnSe shell (**Sample #8):** Te doped CdSe core nanocrystals were prepared using a procedure modified from a previous report[9]. A 50 ml round bottom flask was loaded with 26 mg (0.2 mmol) CdO, 127 mg TDPA and 3.6 g TOPO. After degassing under vacuum for 2 hours at 130°C the temperature was raised to 340°C under argon until CdO dissolved and solution became clear. A Se/Te precursor solution in TOP was prepared by dissolving 40 mg (0.5 mmol) Se in 0.6 ml TOP and mixing in 100 µl of a 0.1 M Te:TOP solution (Te constitutes 4% of the Cd). Reaction solution was heated to 360°C for injection of the Se/Te precursor. The heating mantle was removed immediately after injection. The solution color changed within 10 seconds to a deep dark red shade.

Seeded growth of CdS: A slight modification of previously reported methods[3] was used. A 50 ml round bottom flask was loaded with 100 mg (0.75 mmol) CdO, 600 mg ODPA, 80 mg HPA and 3.6 g TOPO. The reaction flask was degassed for 3 hours at 130°C and then temperature was raised to 330-350°C to dissolve CdO at which point 1.8 ml TOP was added. The CdSe(Te) quantum dots (QDs) were separated and purified for reaction by mixing 1 ml of the QD solution with toluene until completely clear and precipitating with excess acetone. Further purification entailed re-dissolving in 1 ml chloroform/octylamine (6:1) and precipitating with acetone, then re-dissolving in 0.5 ml chloroform/oleic acid/TOP (1:1:8). The QD solution containing ~9×10^{-8}moles of core QDs, was then mixed with an S:TOP solution containing 115 mg S in 1.5 ml TOP. The QD/S solution was quickly injected into the flask at 350°C. A portion of the reaction solution was extracted within 20 seconds for quenching in room temperature ODE.

Continued shell growth of CdZnS: A 50 ml round bottom flask was charged with 1.78 g ODA, 1 ml HDA and 4ml ODE and degassed under vacuum for 4 hours. The CdSe(Te)/CdS NCs QDs were separated for reaction by mixing 2 ml mother solution with chloroform until completely clear and precipitating with excess acetone/ methanol (1:1) after which they were re-dissolved in 1 ml toluene/TOP (1:1). Preparation of S, Cd and Zn precursor solutions is described below (stock solutions section). Cd and Zn oleate solutions were mixed in a 1:2.5 ratio in order to get partial incorporation of Zn in the CdS lattice. Total volumes of 2.6 ml Cd/Zn precursor and 2.6 ml S precursor were added drop-wise to reaction solution over the course of 11 hours. The additions were carried out in a staggered fashion at temperatures ranging from 190° to 220° C.

Continued growth of CdZnSe: Growth of CdZnSe was carried out at 200-220°C by the drop wise addition of

Se:TOP stock solution over the course of about 1 hour. Within 10 min, a new narrow peak in the emission spectrum appeared at 580 nm, indicating that the solution contained large amounts of unreacted Cd and Zn precursors. As growth of ZnSe continued, the two peaks remained completely distinguishable as both peaks red-shifted in tandem. It was also apparent that the VIS emission was getting stronger on the expense of the NIR emission.

Stock solutions for sample #8: Stock solutions of Cd, S, Se, Te and Zn with a concentration of 0.1M for shell growth were prepared in advance; for preparation of Cd (or Zn) oleate 0.1 M - CdO (or ZnO) and oleic acid (ratio of 1:8) were placed in 35 ml ODE in a 100 ml round bottom flask. The solution was degassed for 20 min at 120°C then heated to 300°C on a Schlenck line until full dissolution of the CdO, evident by the solution turning colorless. For S:ODE 0.1 M, 160mg elemental sulfur (5 mmol) and 50ml ODE were placed in a 100 ml round bottom flask. The solution was degassed for 20 min at 120°C and then heated to 200°C for 1 hour, by which time all the sulfur dissolved and the solution attained a yellowish tint. Te:TOP and Se:TOP solutions were prepared by sonicating under heat the desired amount of the elemental material in TOP until it dissolved. For shell growth we applied the technique of successive ion layer deposition and adsorption (SILAR) as described previously[10].

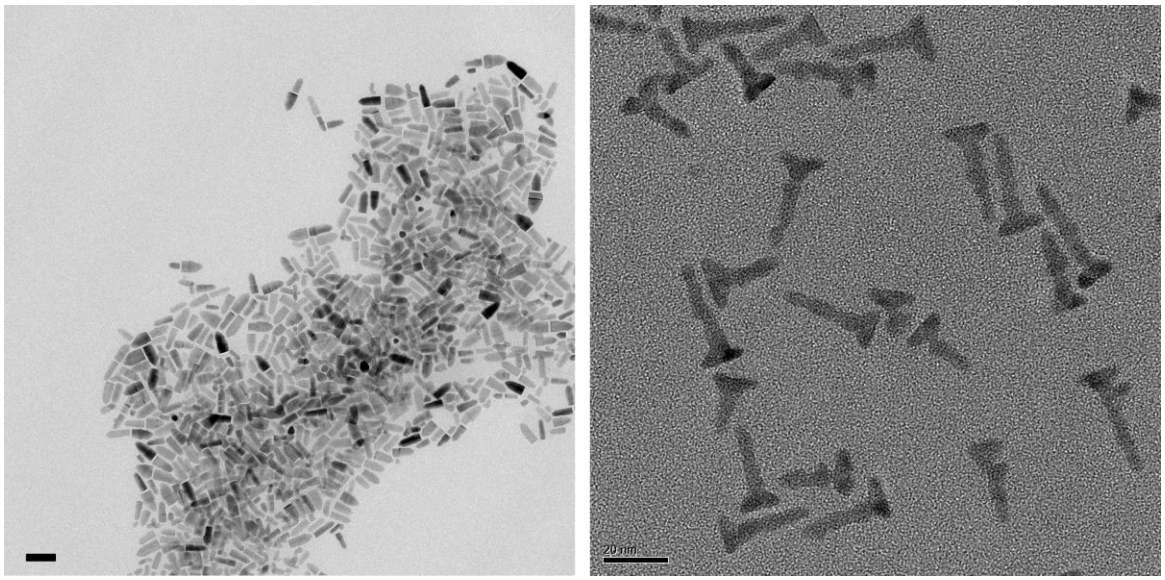

Figure S1. TEM micrographs a. Sample #7 (Scale bar is 50nm.) **b.** Sample #8 (Scale bar is 20nm.)

Table S1 | Statistical size characterization of sample #1 - #8 (Unit is nm).

Sample	#1	#2	#3	#4	#5	#6	#7	#8
Length	7.7±0.9	43.4±7.9	12.8±1.5	29.0±2.1	5.0±0.8	6.0±0.9	33.7±4.2	28.0±4.9
Width	2.9±0.3	4.2±0.4	3.7±-0.4	4.0±0.4			12.1±2.3	5.0±0.4

SI-2. Pattern of the Interdigitated electrode

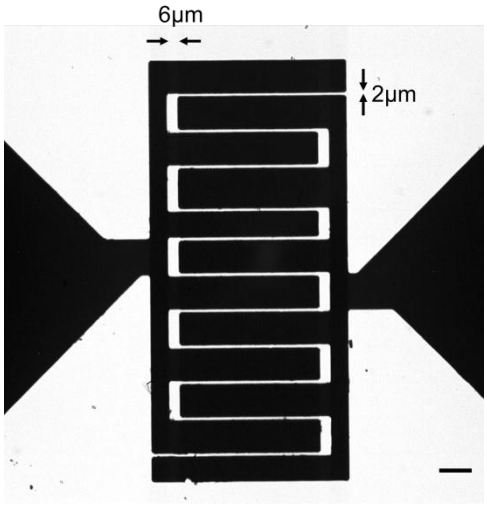

Figure S2. Interdigitated electrode. (bright field image). Electrode spacing is 2μm. Scale bar is 10μm.

Photolithographically patterned interdigitated electrodes (Figure S2) were fabricated at the UCLA Nanoelectronics Research Facility using a home-made designed mask and conventional lithographic and acetone-based lift-off procedures. 100 nm/5 nm Au/Cr layers were deposited onto 25 mm diameter cover glass slides (Circle #1, 0.13 to 0.17mm thickness) using a CHA Mark 40 e-beam evaporator. The gap between finger electrodes is 2um.

SI-3. AC dielectrophoresis NR alignment

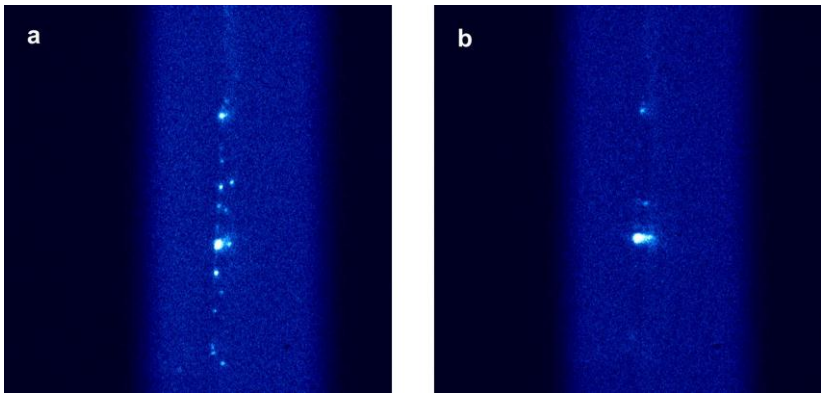

Figure S3. Emission of aligned sample #4 after AC dielectrophoresis. Emission is passed through Glan-Thompson prism (GTP). a, GTP is installed so that NRs' emission polarization is analyzed parallel to the electric field. **b**, GTP is installed so that NR's emission polarization is analyzed perpendicular to the electric field.

NPs samples were dissolved in toluene solution (1mg/ml), diluted ×10, ×100, ×1000 and ×10000 times and casted

onto an interdigitated electrode-patterned cover glass (Figure S2). Sample casting started with the lowest concentration and step-wise increased with higher concentrations to reach optimal surface density for subsequent single molecule spectroscopy (in order to avoid signal overlap on the camera). A dielectrophoresis method was used for each casted layer in an attempt to align NRs long-axis along the field direction[11] (except for control experiments) in order to

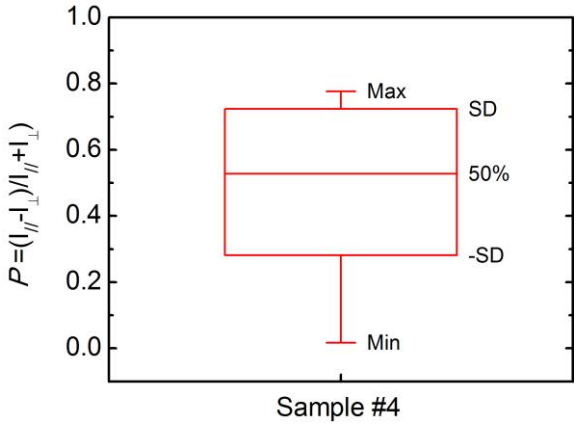

Figure S4. Box chart of 15 NRs' (sample #4) fluorescence polarization. SD is one standard deviation.

maximize the QCSE signal. It was achieved by applying an AC electric field (10 kHz, 100 kV/cm) during the casting process (before toluene evaporation[11]). Figure S3 shows the effect of AC dielectrophoresis on NRs alignment. Since NRs exhibit linear polarization along their long axis[12], their degree of alignment could be assessed by analyzing their polarized emission parallel and perpendicular to the direction of the aligning AC field. The figure shows a field of view containing several NPs of sample #4 after the alignment protocol has been implemented. More bright spots can be seen when the GTP polarization analyzer is aligned parallel to the field (a). Fewer (and weaker) spots are seen when the GTP polarization analyzer is aligned perpendicular to the field (b). By measuring the parallel $I_{\parallel}$ and perpendicular $I_{\perp}$ polarization components of individual NRs' emission, one can calculate the polarization P according to: $P = (I_{\parallel} - I_{\perp})/(I_{\parallel} + I_{\perp})$ for each NR. Figure S4 shows a box chart of P values for 15 individual NRs. The mean P is 0.50, suggesting a reasonable alignment yield (random orientation would have resulted in an average $\bar{P} = 0$), a slightly lower value than the one reported for CdSe NR in ref. [12].

SI-4. Optical setup

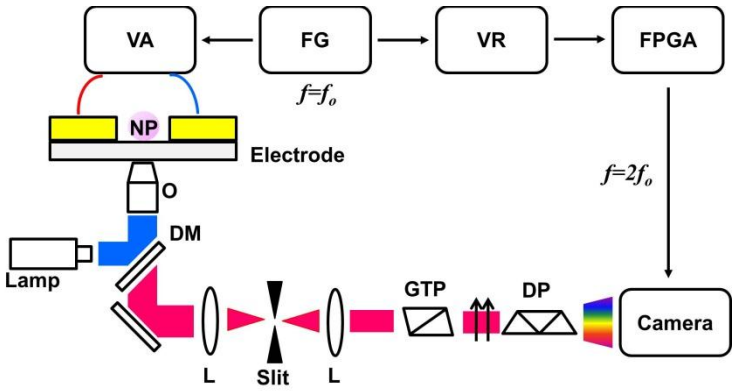

Figure S5. Schematics of the set up used to perform single nanoparticle QCSE spectroscopy. (L=lens, GTP=Glan-Thompson prism, DP=dove prism, DM=dicroic mirror, FG=function generator, NP=nanoparticle, O=objective lens, FPGA=field-programmable gate array, VR=voltage regulator, VA=voltage amplifier)

Figure S5 describes the set-up used to acquire QCSE spectroscopic data on single QDs and NRs. The set-up is based on an Olympus IX71 inverted microscope equipped with a Xenon lamp (Olympus, U-LH75XEAPO, 75W) and excitation filter (BP 470/40, Chorma Technology Corp, Bellows Falls, VT). The emission of the NPs is collected by ×60 objective lens (Olympus, PlanApo 60×, n=1.45, oil immersion), passed through a dichroic mirror (DM, 505DCXRU, Chorma Technology Corp, Bellows Falls, VT) and then directed to the high resolution spectral detection arm. Spectral features (Figure S6a) are selected by a variable slit (in order to remove overlapping spectra of neighboring NPs; Figure S6). A Glan-Thompson prism (GTP, Thorlabs, Newton, NJ, acting as a linear polarizer downstream from the slit) selects NRs that are aligned along the direction of the applied electric field. Larger QCSE wavelength shifts are expected for charge separation along the long axis of the NR, which is also the direction of its polarized emission[12]. The emission is then dispersed by a dove prism (DP, Thorlabs, Newton, NJ) and detected by an Andor iXon electron multiply (EM) charge coupled device (CCD) camera (EMCCD, Andor iXon, South Windsor, CT) (see also Figure S6c). The horizontal axis of the resulted spectral images was calibrated with 532 nm (DPGL-20P, World Star Tech, Toronto, Canada), 594 nm (25 LYP 173, Melles Griot, Albuquerque, NM) lasers and 810 nm LED (NT59-432, Edmund optics, Barrington, NJ) lines using a quadratic fit.

SI-5. Data Analysis

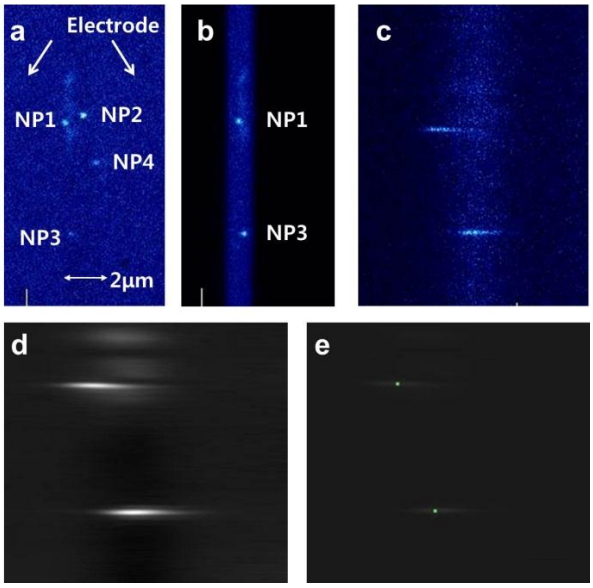

Figure S6. The procedure used to acquire spectral images. a, NPs image (single frame) taken without the slit and the prism; **b,** the same image taken with the slit; **c,** same image as in **b** after dispersion by the prism; **d**, Average of 200 frames of the image in **c** after background correction; **e,** automated spectral peak detection (overlaid with **d**). Green dots represent spectral peak positions of NP1 and NP3.

Figure S6 illustrates the procedure that was utilized to find NPs, select isolated NPs, and acquire their spectra. For example, four NPs located in the gap between two electrodes' fingers were observed in the data set shown in Figure S6a (NP1-NP4). Since the dispersed emission of NP2 overlapped with that of NP1, the variable slit was adjusted to filter-out signals from NP2 and NP4, *i.e*. only the signals from NP1 and NP3 were selected for further analysis (Figure S6b). After passing through the dispersive prism, the two spectra of NP1 and NP3 were recorded on the EMCCD (Figure S6c). The camera acquisition clock (frame-rate) was synchronized to the alternation frequency of the (quasi) DC electric field (square wave, typically f_o=5 Hz) that was applied to the interdigitated electrodes using a function generator (FG2A, Beckman industrial, Fullerton, CA) followed by a voltage regulator and a high voltage amplifier (STM 100 controller, RHK technology, Troy, MI). The amplitude of the applied field to the electrodes could reach up to ±500 kV/cm (f=5 Hz). The function generator synchronization signal was frequency doubled by a Labview-controlled FPGA board (f= 2f_o= 10 Hz) (Spartan 3E, Xilink, San Jose, CA) resulting in successive synchronized acquisitions of camera frames in the V_{on} and V_{off} periods of the square wave (the delays between the generated waveform by the function generator, the high-voltage amplifier, and the actual applied voltage on the electrodes, were confirmed to be negligible; the RC time constant of the electrode was measured to be 0.2 ps). Typical data set was acquired for 20~30 seconds in a format of a movie of ~200-300 alternating frames, *i.e*. 100~150 frames for each V_{on} and V_{off}.

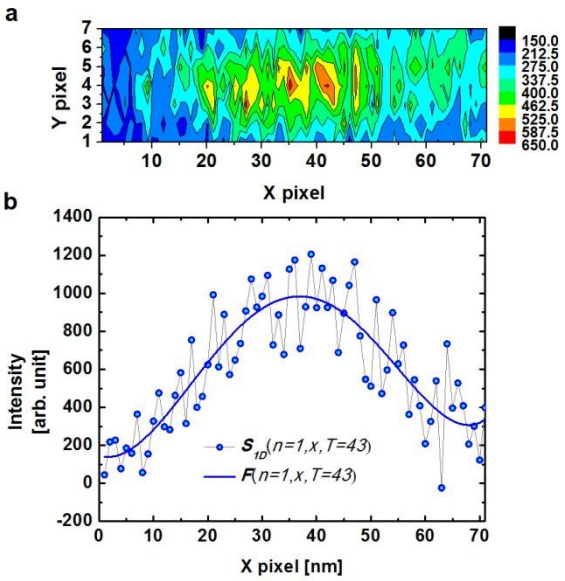

Figure S7. Intensity profile of the 43th frame in a movie of NP1 in Figure S6. a, 2 dimensional intensity profile S_{2D}(n=1,x, y, t=43). Color map illustrates photon number acquired at each pixel. **b,** 1D intensity profile S_{1D}(n=1,x,t=43) and its fitting curve (*F*)

All data sets were automatically analyzed using a home-written Matlab program. The program detects NPs location in the field-of-view (on the sum of all movie frames, Figure S6e) and extracts, for each frame in a movie, all relevant parameters from individual spectrum including the peak emission wavelength (λ_{peak}), the integrated intensity, and the full width half maximum (FWHM). It then calculates the histograms of these properties for all V_{on} and V_{off} frames in a movie. To achieve this, the following steps were performed:

(i) Background correction: Owing to the nonlinear prism's dispersion (especially at λ > 700nm) and random background noise, background was corrected across the whole field (Figure S6d). The X-axis (column) of the raw spectral image represents wavelength. The Y-axis (row) of the raw spectral image represents real space. All pixels in the field-of-view were integrated over all frames (along t) to average out temporal intensity fluctuations, and over all rows (Y-axis) to achieve an averaged, 'single row' background. This vector is then subtracted from each frame and each row to achieve background correction.

(ii) Peak detection: The spectrum of a single NP spreads over several rows and columns. To detect each spectrum's peak position, a Matlab built-in one-dimensional peak detection function, 'findpeaks', was implemented twice, both for X and for Y directions. It returns the peak coordinates (x_n, y_n, where *n* indexes individual NPs). When the areal concentration of NPs was adjusted properly (~1 NP per 10 μm^2), the yield of spectra extraction from individual NPs approached 95%.

(iii) Spectrum's profile and thresholding: The program returned a list of NPs coordinates (x_n, y_n), (Figure S6e) and subsequently extracted parameters for all NPS in the list, one NP at a time. For each individual NP's spectrum of each frame, a profile is defined: S_{2D}(n, x, y, t), with index *n*, frame *t* and peak position (x_n, y_n) in the region of

interest (ROI). Figure S7a is a representative 2D spectrum profile of the 43th frame of NP1 in Figure S6: $S_{2D}(1,x,y,43)$. Only frames with NPs in the blinking-on state are retained (from the full set of 200~300 frames) by applying a threshold filter. The threshold (*Th*) is defined as the mean value of the total integrated intensity of individual NP, $Th(n)=\frac{1}{T}\sum_{t,x,y} S_{2D}(n,x,y,t)$ where T is the total length of the movie. Signals of frames with total integrated intensity $\left(=\sum_{x,y} S_{2D}(n,x,y,t)\right)$ larger than *Th* are retained and their spectrum is reduced to a 1D spectrum profile by integrating over the Y-axis: $S_{1D}(n,x,t)=\sum_{y} S_{2D}(n,x,y,t)$. $S_{1D}(n,x,t)$ is then fitted by a 7th order polynomial $F(n,x,t)$ (since spectra were not fitted well by Gaussians or Lorentzians). Figure S7b shows S_{1D} for the data shown in Figure S7a.

(iv) Final data reduction and presentation: S_{1D} and F data (excluding blinking-off frames) are further divided into V_{on} and V_{off} frames which are used for the construction of average spectra (as in Figures. 1c, 2c, 3c) by averaging $S_{1D}(n, x, t)$ and the construction of spectral peak position histograms (Figures. 1d, 2d, 3d) by tabulating peak positions (x_{peak}) of $F(n, x, t)$ for V_{on} and V_{off} frames respectively. Finally, the X-axis is converted to wavelength by quadratic fitting to the calibration data (taken with 2 lasers and 1 LED spectral lines,). The differential spectrum (Figure 1e, 2e, 3e) is acquired by subtracting V_{off} averaged spectrum from V_{on} averaged spectrum.

SI-6. Simulations

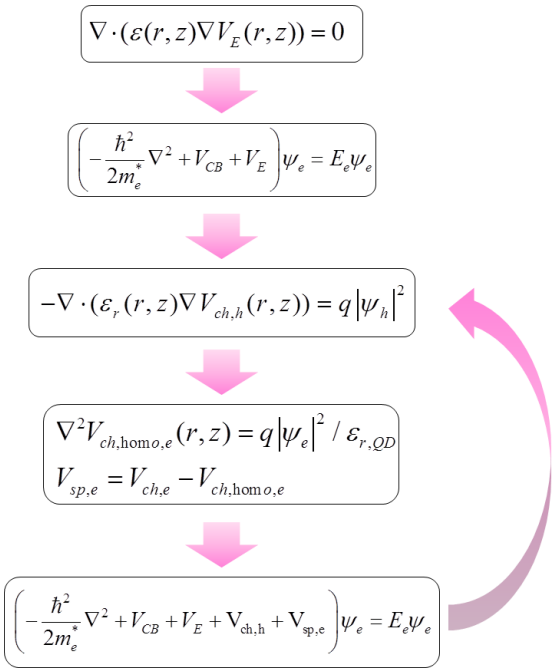

Figure S8. Quantum calculation flow chart

We calculated the QCSE by solving the self-consistent Schrödinger-Poisson equations using a home-written Matlab program. Cylindrical symmetry was employed using a finite difference mesh. On every discretized mesh point, Schrödinger and Poisson equations were solved by assuming effective masses and self-consistent field approximation. The code generates electron's and hole's energy levels, overlap integral, and exciton binding energy by solving the coupled Schrödinger-Poisson equations iteratively using the finite difference method. To achieve three dimensional calculation with manageable computational effort, we apply axial (cylindrical) symmetry to the geometry and Laplacian operators for homogeneous space (or gradient and divergence operators for inhomogeneous space) in the coupled equations. The entire computational space extends 3~5nm further from the NP boundary (allowing for e and h wavefunctions to extend outside of the NPs' boundaries and decay into free space). Figure S8 presents the flow diagram for these calculations. First we define geometry and geometry-dependent parameters such as effective masses (m*(r,z)), dielectric constants (ε_r(r,z)), and conduction and valence band profiles (V_{CB} and V_{VB}). Parameters and their references used in this calculation are summarized at Tables S2 and S3. At the NP boundary, ε_r is assigned the average value of the NP and air dielectric constants. The potential generated by the external electric field (V_E) is calculated by solving the Laplacian equation $\nabla\cdot(\varepsilon_r(r,z)\nabla V_E(r,z))=0$ with the boundary condition: (V_E(z=0)=0, V_F(z=d)=qF×d), where F is the electric field, and d is the total length of the computational space. With these potentials at hand, the Schrödinger equations for the electron:

$$\left(-\frac{\hbar^2}{2m_e^*}\nabla^2+V_{CB}+V_E\right)\psi_e=E_e\psi_e$$

and for the hole: $$\left(-\frac{\hbar^2}{2m_h^*}\nabla^2 + V_{VB} - V_E \right)\psi_h = E_h\psi_h$$

are solved next (using the Dirichlet boundary conditions). After normalization of the wavefunctions, the Poisson equation $-\nabla\cdot(\varepsilon_r(r,z)\nabla V_{ch,h}(r,z)) = q\left|\psi_h\right|^2$ is solved (with a Dirichlet boundary condition) to derive the hole coulomic potential $V_{ch,h}$. The electron coulomic potential $V_{ch,e}$ is obtained in a similar way. In addition to the potential generated from the other particle, each particle is influenced by its own self-polarization potential ($V_{sp,e}$, $V_{sp,h}$)[13,14] arising from the dielectric mismatch with its surrounding. $V_{sp,e}$ is calculated using: $V_{sp,e} = V_{ch,e} - V_{ch,homo,e}$ and $V_{ch,homo,e}$ is calculated using: $\nabla^2 V_{ch,homo,e}(r,z) = q\left|\psi_e\right|^2 / \varepsilon_{r,QD}$. $\varepsilon_{r,QD}$ is the dielectric constant of the NP (which has a constant value). $V_{sp,h}$ is obtained similarly. With these potentials, Schrödinger equations are solved again for *e* and *h* with all of the contributions to the potentials:

$$\left(-\frac{\hbar^2}{2m_e^*}\nabla^2 + V_{CB} + V_E + V_{ch,h} + V_{sp,e} \right)\psi_e = E_e\psi_e$$

$$\left(-\frac{\hbar^2}{2m_h^*}\nabla^2 + V_{VB} - V_E + V_{ch,e} + V_{sp,h} \right)\psi_h = E_h\psi_h$$

This process is repeated iteratively until the electron (or/ and hole) energies converge. In most cases, four iterations are sufficient to obtain a convergence error of $\Delta E_e/E_e \leq 0.1\%$.

SI-7. Dimensions and parameters used in the simulations

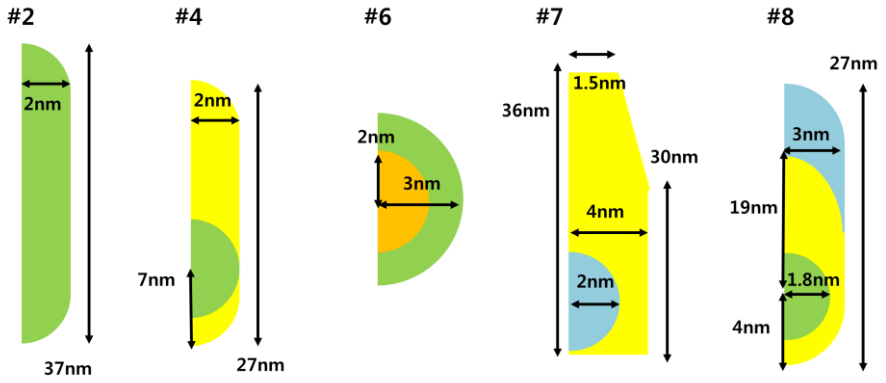

Figure S9. Simulated geometries for samples #2, #4, #6, #7, #8. CdSe (green), CdS (yellow), CdTe (orange), ZnSe (#7, cyan), CdZnSe (#8, cyan)

Geometries used for simulation are shown in Figure S9. Parameters used in this study were obtained from the literature[15,16,17,18] and are summarized in Table S2 and S3. For simplicity, the same dielectric constant (ε_r=9) was applied for the all samples, and the dielectric constant of air (ε_r=1) was assumed for the immediate surroundings of the NP. Conduction band (Δ_e) offset between CdS-CdZnSe is assumed to have 0.3eV which is a medium value of CdSe-CdS and ZnSe-CdS. Valence band offsets (Δ_e) of sample #8 are assumed to be zero except CdS-CdZnSe interface in order to ignore type-I transition and only take account type-II transition.

	CdSe	CdTe	CdS	ZnSe
m^*_e	0.13	0.11	0.2	0.14
m^*_h	0.45	0.35	0.7	0.53

Table S2. Electron and hole effective masses

	CdSe-CdTe	CdSe-CdS	CdS-ZnSe
Δ_e	0.42	0.2	0.8
Δ_h	-0.57	0.78	-0.52

Table S3. Conduction and valence band offsets. For example, Conduction band edge of CdTe is 0.42eV higher than CdSe. Unit is eV.

SI-8. Wavelength shift (Δλ) histograms

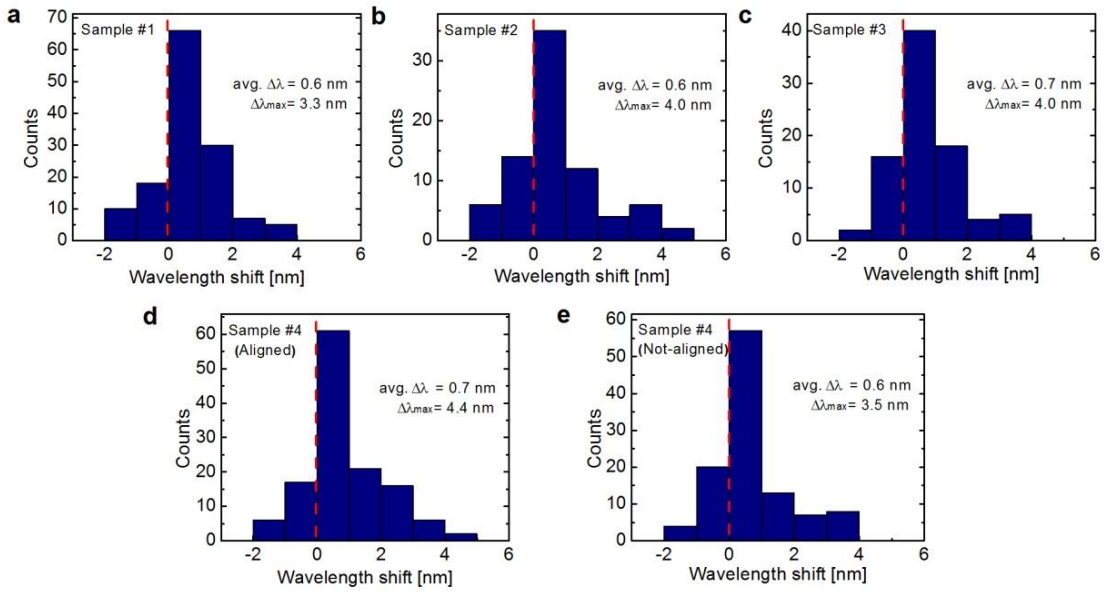

Figure S10. Wavelength shift (Δλ) histograms for: **a,** Sample #1; **b,** Sample #2; **c,** Sample #3; **d,** Sample #4; **e,** Sample #4; Measurements (**a~d**) are for aligned samples. **e,** non-aligned Sample #4 (serving as a control).

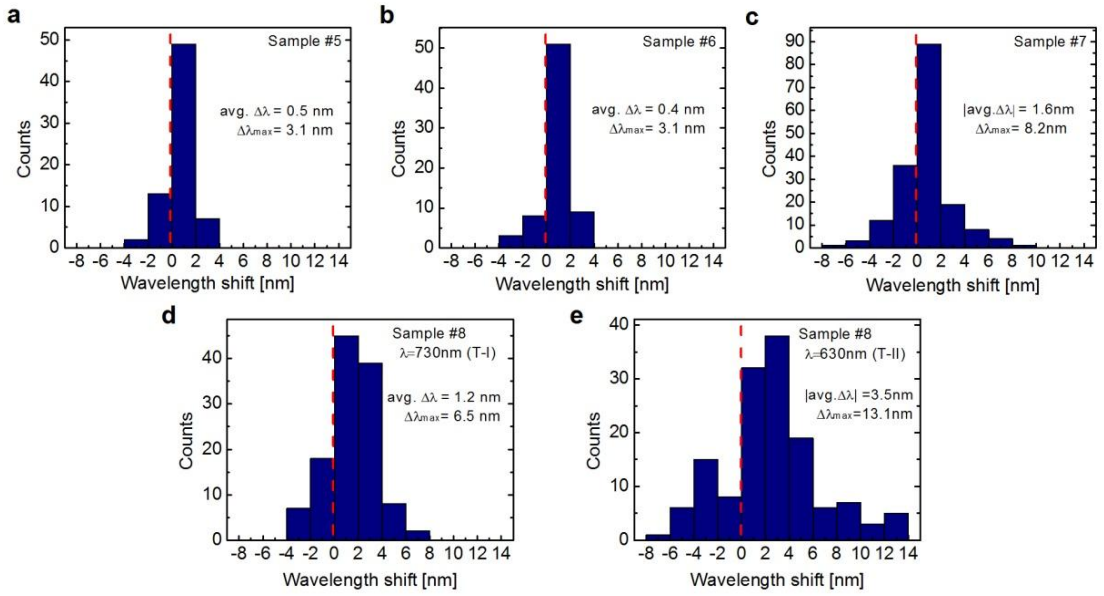

Figure S11. Wavelength shift (Δλ) histograms for **a,** Sample #5 **b,** Sample #6 **c,** Sample #7 **d,** Sample #8, type-I transition **e,** Sample #8, type-II transition.

SI-9. Spectrum of sample #8.

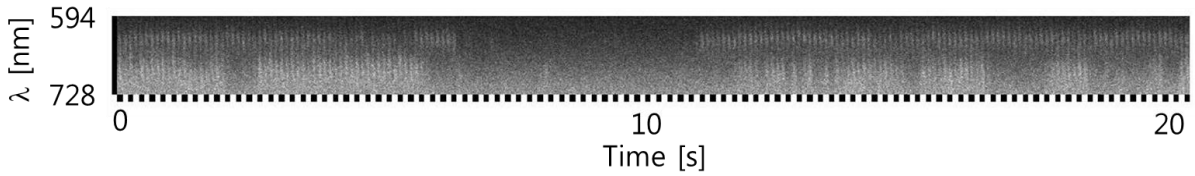

Figure S12. Dual-color spectra of sample #8. Type-II transition (top), and type-I transition (bottom) as function of field modulation.

References

1. Wang, W.; Banerjee, S.; Jia, S.; Steigerwald, M. L.; Herman, I. P. Ligand Control of Growth, Morphology, and Capping Structure of Colloidal CdSe Nanorods. *Chem. Mater.* **2007,** *19*, 2573-2580.
2. Carbone, L.; Nobile, C.; De Giorgi, M.; Sala, F. D.; Morello, G.; Pompa, P.; Hytch, M.; Snoeck, E.; Fiore, A.; Franchini, I. R. *et al.* Synthesis and Micrometer-Scale Assembly of Colloidal CdSe/CdS Nanorods Prepared by a Seeded Growth Approach. *Nano Lett.* **2007,** *7*, 2942-2950.
3. Talapin, D. V.; Nelson, J. H.; Shevchenko, E. V.; Aloni, S.; Sadtler, B.; Alivisatos, A. P. Seeded Growth of Highly Luminescent CdSe/CdS Nanoheterostructures with Rod and Tetrapod Morphologies. *Nano Lett.* **2007,** *7*, 2951-2959.
4. Jack Li, J.; Tsay, J. M.; Michalet, X.; Weiss, S. Wavefunction Engineering: From Quantum Wells to Near-infrared Type-II Colloidal Quantum Dots Synthesized by Layer-by-layer Colloidal Epitaxy. *Chem. Phys.* **2005,** *318*, 82-90.
5. Hewa-Kasakarage, N. N.; Kirsanova, M.; Nemchinov, A.; Schmall, N.; El-Khoury, P. Z.; Tarnovsky, A. N.; Zamkov, M. Radiative Recombination of Spatially Extended Excitons in (ZnSe/CdS)/CdS Heterostructured Nanorods. *J. Am. Chem. Soc.* **2009,** *131*, 1328-1334.
6. Deutsch, Z.; Schwartz, O.; Tenne, R.; Popovitz-Biro, R.; Oron, D. Two-Color Antibunching from Band-Gap Engineered Colloidal Semiconductor Nanocrystals. *Nano Lett.* **2012,** *12*, 2948-2952.
7. Talapin, D. V.; Koeppe, R.; Götzinger, S.; Kornowski, A.; Lupton, J. M.; Rogach, A. L.; Benson, O.; Feldmann, J.; Weller, H. Highly Emissive Colloidal CdSe/CdS Heterostructures of Mixed Dimensionality. *Nano Lett.* **2003,** *3*, 1677-1681.
8. Dorfs, D.; Salant, A.; Popov, I.; Banin, U. ZnSe Quantum Dots Within CdS Nanorods: A Seeded-Growth Type-II System. *Small* **2008,** *4*, 1319-1323.
9. Avidan, A.; Deutsch, Z.; Oron, D. Interactions of Bound Excitons in Doped Core/shell Quantum Dot Heterostructures. *Phys. Rev. B* **2010,** *82*, 165332.
10. Li, J. J.; Wang, Y. A.; Guo, W.; Keay, J. C.; Mishima, T. D.; Johnson, M. B.; Peng, X. Large-Scale Synthesis of Nearly Monodisperse CdSe/CdS Core/Shell Nanocrystals Using Air-Stable Reagents *via* Successive Ion Layer Adsorption and Reaction. *J. Am. Chem. Soc.* **2003,** *125*, 12567-12575.
11. Hu, Z.; Fischbein, M. D.; Querner, C.; Drndić, M. Electric-Field-Driven Accumulation and Alignment of CdSe and CdTe Nanorods in Nanoscale Devices. *Nano Lett.* **2006,** *6*, 2585-2591.
12. Hu, J.; Li, L.-s.; Yang, W.; Manna, L.; Wang, L.-w.; Alivisatos, A. P. Linearly Polarized Emission from Colloidal Semiconductor Quantum Rods. *Science* **2001,** *292*, 2060-2063.
13. Boda, D.; Gillespie, D.; Nonner, W.; Henderson, D.; Eisenberg, B. Computing Induced Charges in Inhomogeneous Dielectric Media: Application in a Monte Carlo Simulation of Complex Ionic Systems. *Phys. Rev. E* **2004,** *69*, 046702.
14. Movilla, J. L.; Climente, J. I.; Planelles, J. Dielectric Polarization in Axially-symmetric Nanostructures: A Computational Approach. *Comput. Phys. Commun.* **2010,** *181*, 92-98.
15. Wang, C. H.; Chen, T. T.; Tan, K. W.; Chen, Y. F.; Cheng, C. T.; Chou, P. T. Photoluminescence Properties of CdTe/CdSe Core-shell Type-II Quantum Dots. *J. Appl. Phys.* **2006,** *99*, 123521-4.
16. Baskoutas, S.; Terzis, A. F. Size-dependent Band gap of Colloidal Quantum dots. *J. Appl. Phys.* **2006,** *99*, 013708-4.
17. Nemchinov, A.; Kirsanova, M.; Hewa-Kasakarage, N. N.; Zamkov, M. Synthesis and Characterization of Type II ZnSe/CdS Core/Shell Nanocrystals. *J. Phys. Chem. C* **2008,** *112*, 9301-9307.
18. Mews, A.; Eychmueller, A.; Giersig, M.; Schooss, D.; Weller, H. Preparation, Characterization, and Photophysics of the Quantum Dot Quantum Well System Cadmium Sulfide/Mercury Sulfide/Cadmium Sulfide. *J. Phys. Chem.* **1994,** *98*, 934-941.